EFFECTS OF AIR-BRIDGES AND MITERING ON COPLANAR WAVEGUIDE 90° BENDS: THEORY AND EXPERIMENT

A. A. Omar *, Y. L. Chow *, L. Roy ** and M.G. Stubbs **

* Department of Electrical and Computer Engineering
University of Waterloo, Waterloo, Ont., Canada, N2L 3G1

** Communications Research Center
Ottawa, Ont., Canada, K2H 8S2

ABSTRACT

The effects of the mitres and air-bridge dimensions and locations on coplanar waveguide (CPW) 90° bends are investigated using the moment method. An experiment is conducted to verify the accuracy of our calculations. These show that the CPW bends are mainly affected by the air-bridge height and location not the mitering.

I. INTRODUCTION

An important obstacle facing coplanar waveguide (CPW) is the lack of theoretical investigation of many important CPW discontinuities like bends and T-junctions. Such discontinuities are the building blocks of larger CPW circuits. So far, there is no detailed investigation of the CPW 90° bend. Some results on this bend were provided by Jansen [1], in the description of his simulator for CPW circuits, using a quasi static model for the air-bridges. This model, however, is potentially inaccurate at high frequencies.

In this paper, we investigate the effects of mitering and air-bridge dimensions and locations, on the S-parameters and on the power loss due to radiation and surface waves in the CPW 90° mitered and non-mitered bends shown in Fig.1a,b. Air-bridges placed near CPW discontinuities can reduce the parasitic slot-line mode which tends to radiate. The method used in this paper was developed in [2], and is based on the mixed potential integral equation technique with the moment method and the computationally efficient full wave *complex image Green's functions* [3]. An experiment was conducted to verify the accuracy of our results on the mitered bend.

Section (II) briefly explains the theoretical formulation for solving the CPW bend with air-bridges. Section (III) provides a comparison between our theoretical and experimental results on the mitered bend. Section (IV) discusses the effects of mitering and air-bridges on the CPW bends.

II. THEORY

As in [2], the duality principle is used to convert the CPW problem with an air-bridge, shown in Fig.2a, into two parallel (dual) electric strip subproblems as shown in Fig.2b,c, with the air-bridge existing only in the upper subproblem. This subproblem is equivalent to parallel strips embedded in free space with a magnetic air-bridge loop, as shown in Fig.2b. The lower subproblem of Fig.2c is equivalent to the dual strips embedded inside a magnetic slab characterized by $\varepsilon_o, \mu_o\mu_r$, with $\mu_r = \varepsilon_r$ of the original problem of Fig.2a.

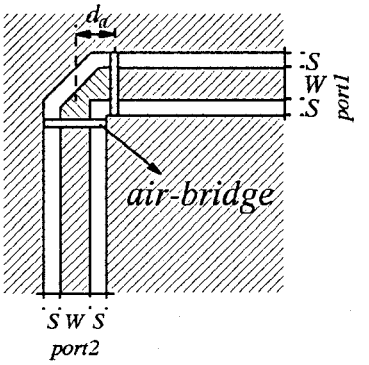

(a)

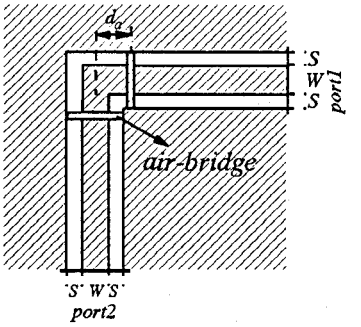

(b)

Fig.1: Top views of the CPW 90° bends.
a) Mitered CPW bend. b) Non-mitered CPW bend.

BB

CH3277-1/93/0000-0823$01.00 © 1993 IEEE

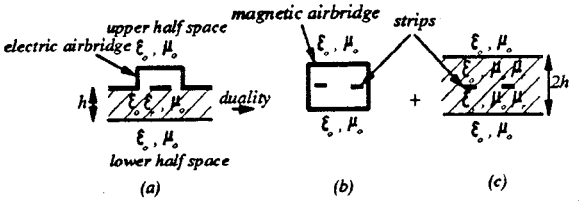

Fig.2: Splitting the CPW problem with air-bridge into two parallel strip subproblems through duality: a) The original CPW problem with air-bridge. b) The upper subproblem. c) The lower subproblem with $\mu_r = \varepsilon_r$.

Applying the boundary conditions on the strips and (dual) air-bridges whose 3-D view is shown in Fig.3, leads to a pair of coupled mixed potential integral equations which is solved using the Galerkin moment method [2]. This yields:

$$\begin{bmatrix} \underline{V}^e \\ \underline{V}^m \end{bmatrix} = \frac{1}{2}\begin{bmatrix} [Z^{(1)}+Z^{(2)}] & [Z^{em}] \\ [Z^{me}] & [Z^m] \end{bmatrix}\begin{bmatrix} \underline{I}^e \\ \underline{I}^m \end{bmatrix} \tag{1}$$

where the factor half in (1) is due to each subproblem in Fig.2 representing a half space. $\underline{I}^e, \underline{V}^e$ are column matrices for the electric currents and voltage excitations on the strips. $\underline{I}^m, \underline{V}^m$ are the corresponding magnetic currents and voltage excitations on the (dual) air-bridges with $\underline{V}^m = \underline{0}$ since there is no magnetic voltage (electric current) excitation on the (dual) air-bridges. $[Z^{(1)}], [Z^{(2)}]$ represent the coupling between the electric current segments of the strips of the upper and lower subproblems, respectively. $[Z^m]$ represents the coupling between the magnetic currents of the (dual) air-bridge and is the dual of $[Z^{(1)}]$. $[Z^{em}], [Z^{me}]$ represent the coupling between the magnetic and electric currents and are related by [2]:

$$[Z^{em}] = -[Z^{me}]^T \tag{2}$$

where superscript T denotes transpose of a matrix.

Finally, Eq. (1) is solved for the electric current on the strips (I^e) from which the S-parameters are calculated using transmission line theory.

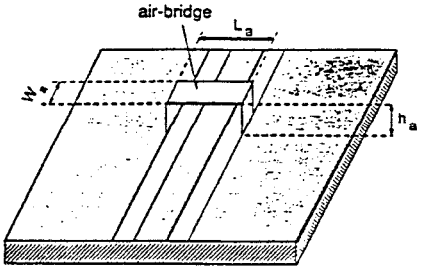

Fig.3: A 3-D view of the CPW with air-bridge.

III. EXPERIMENTAL VERIFICATION

To experimentally verify the accuracy of our method and computer code, measurements were performed on the mitered CPW bend circuit of Fig.4. Very good agreement was obtained between the theoretical and experimental results (obtained from our laboratory), as shown in Fig.5a,b.

IV. NUMERICAL RESULTS AND CONCLUSIONS

With the theoretical method and computer code validated, various parameters of the CPW 90° bend are adjusted to investigate their effects which are briefly summarized below.

A. The mitering slightly reduces $|S_{11}|$ and slightly increases $|S_{21}|$ up to 40*GHz*, as shown in Fig.6. Even if the frequency is increased to 100*GHz*, a very recent numerical test shows that the mitering effect is still minimal.

B. The air-bridge height (h_a) is the dominant factor affecting the bend. Fig.7 shows that increasing h_a causes a substantial decrease in $|S_{11}|$ and an increase in $|S_{21}|$ until almost perfect transmission is achieved for $h_a > 8\mu m$. This is due to the decrease in the air-bridge capacitance as h_a is increased.

C. Increasing the air-bridge width (W_a) causes an increase in $|S_{11}|$ and a decrease in $|S_{21}|$, as shown in Fig.8 for the mitered bend. This is due to the increase in the air-bridge capacitance as W_a is increased.

D. The length of the air-bridge (L_a) was found to have almost no effect on the performance of the CPW bends.

E. The air-bridges should be placed as close as possible to the center of the bend for maximum elimination of the slot-line mode and hence minimum radiation loss due to this mode. This can be inferred from Fig.9, which shows the power loss from radiation and surface waves (in the non-mitered bend) versus air-bridge location d_a at a high frequency of 100*GHz*. At a more normal 40*GHz* this loss was found not to exceed 1%, which is within the range of numerical error of our method.

From the above, we conclude that the air-bridges dimensions and locations should be properly chosen to minimize the reflection and maximize the transmission of the CPW bends, and that mitering a CPW bend is not important.

REFERENCES

[1] R. Bromme and R.H. Jansen, "Systematic investigation of coplanar waveguide MIC/MMIC structures using a unified strip/slot 3D electromagnetic simulator," *IEEE MTT-S Dig.*, 1991, pp. 1081-1084.

[2] A.A. Omar and Y.L. Chow, "A solution of coplanar waveguide with air-bridges using complex images," *IEEE Trans. Microwave Theory and Tech.*, Vol. MTT-40, no. 11, pp. 2070-2077, Nov. 1992.

[3] Y.L. Chow, J.J. Yang, D.G. Fang and G.E. Howard,"A closed form spatial Green's function for thick microstrip substrate," *IEEE Trans. Microwave Theory Tech.*, Vol.MTT-39, no.3, March 1991.

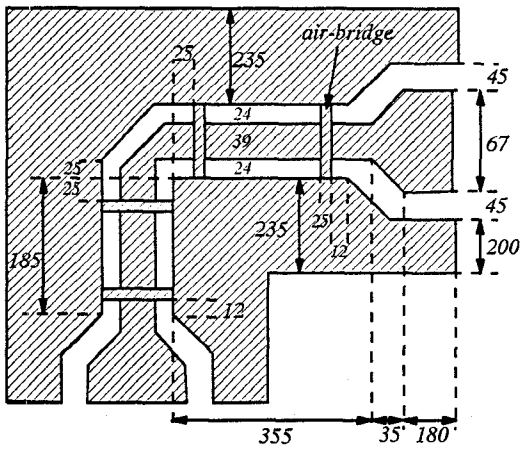

Fig.4: The top view of the *measured* CPW mitered bend with air-bridges and probing pads. ($h = 90\mu m$, $\varepsilon_r = 12.9$, $h_a = 2\mu m$, $W_a = 25\mu m$, $L_a = 87\mu m$). Figure not to scale, and dimensions in μm.

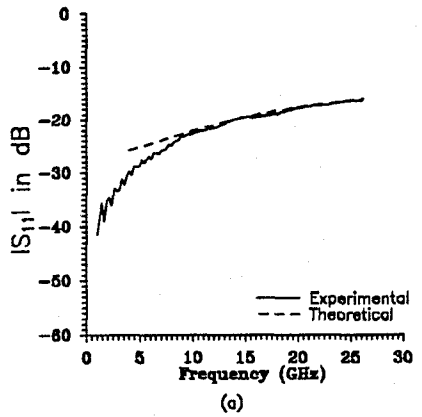

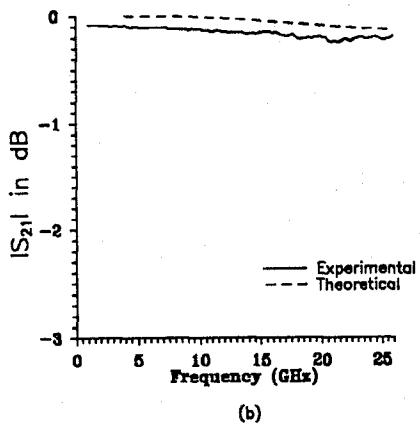

Fig.5: Comparison between the experimental and the theoretical results for the S-parameters of the CPW mitered bend circuit of Fig.4: a) $|S_{11}|$. b) $|S_{21}|$. ($h = 90\mu m$, $\varepsilon_r = 12.9$, $h_a = 2\mu m$, $W_a = 25\mu m$, $L_a = 87\mu m$)

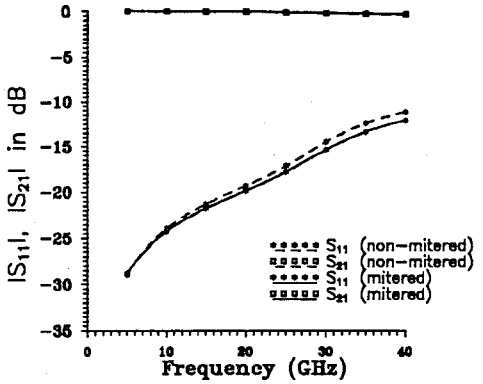

Fig.6: Comparison between the S-parameters of the mitered and non-mitered bends of Fig.1a,b, respectively. ($W = 39\mu m, S = 24\mu m, h = 90\mu m$, $\varepsilon_r = 12.9$, $d_a = 37.5\mu m$, $W_a = 50\mu m$, $h_a = 2\mu m$, $L_a = 87\mu m$)

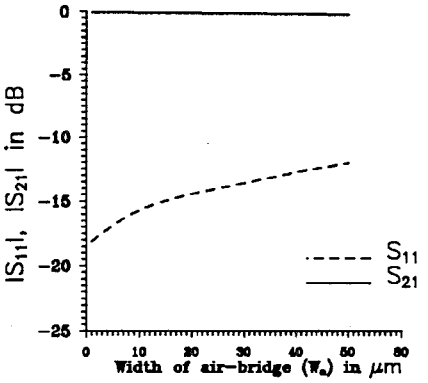

Fig.8: The S-parameters for the CPW mitered bend of Fig.1a versus air-bridge *width* (W_a). ($f = 40GHz$, $W = 39\mu m$, $S = 24\mu m$, $h = 90\mu m$, $\varepsilon_r = 12.9$, $d_a = 37.5\mu m$, $h_a = 2\mu m$, $L_a = 87\mu m$)

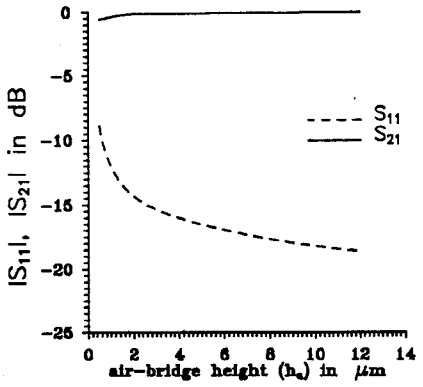

Fig.7: The S-parameters for the CPW mitered bend of Fig.1a versus air-bridge *height* (h_a). ($f = 40GHz$, $W = 39\mu m$, $S = 24\mu m$, $h = 90\mu m$, $\varepsilon_r = 12.9$, $d_a = 37.5\mu m$, $W_a = 25\mu m$, $L_a = 87\mu m$)

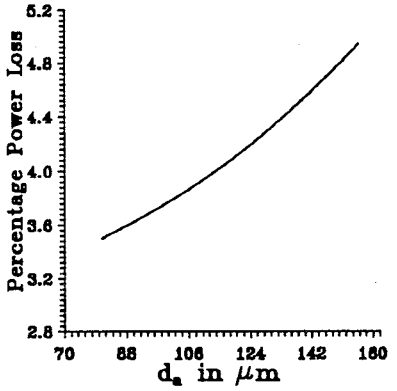

Fig.9: The percentage power loss versus the air-bridge location (d_a) for the non-mitered CPW bend of Fig.1b. ($f = 100GHz$, $W = 39\mu m$, $S = 24\mu m$, $h = 90\mu m$, $\varepsilon_r = 12.9$, $L_a = 87\mu m$, $W_a = 25\mu m$, $h_a = 2\mu m$)